JTTEE 3:169-178

Wear and Erosion Behavior of Plasma-Sprayed WC-Co Coatings

H.J. Kim, Y.G. Kweon, and R.W. Chang

Wear mechanisms of air plasma-sprayed WC-12%Co coatings were studied by using a dry sand rubber wheel (DSRW) abrasive, ring-on-square adhesive wear, and alumina particle erosion tests. Coating properties such as intersplat cohesive strength, porosity, surface roughness, hardness, and retained carbide as well as microstructures were characterized to assess their relationship on wear performance. Porosity, hardness, surface roughness, and retained carbide of the coatings are not the principal factors affecting wear performance. Intersplat cohesive strength of coatings, measured by a simple bonding test, is the most significant factor that relates to the wear rate of thermal spray coatings.

1. Introduction

THERMAL sprayed WC-Co coatings have been widely used for many aerospace and industrial applications. The principal function of these coatings is to resist severe environments for such wear mechanisms as abrasion, adhesion, and particle erosion. A considerable amount of work has been undertaken to optimize coating properties and wear performance. Coating properties (bond strength, porosity, hardness, surface roughness, etc.) depend on starting powder characteristics (size, shape, composition, and manufacturing method), as well as spraying methods and process parameters.[1-12] Vacuum plasma spray (VPS), high-energy plasma (HEP), and high-velocity oxygen fuel (HVOF) processes have been developed to obtain reduced porosity, higher hardness, and improved intersplat cohesion of the coating.[1,2,6,7] However, it is difficult to use the spraying process to produce consistent quality WC-Co coatings because of the complex chemical and physical transformations occurring in the plasma stream, which significantly affect the properties of the coatings. Therefore, it is necessary to determine which coating properties are the principal factors for practical industrial applications.

It is generally accepted that optimum wear properties must retain a large volume fraction of finely distributed tungsten monocarbide.[4,13] Porosity, surface roughness, and hardness of the coating are not the main factors affecting wear performance.[1,14-17] Microstructural features such as the lamellar structure of coatings and the effect on wear have not received sufficient attention until recently. By examining the surface morphologies of the splats, Furukubo et al. have shown that adhesive wear resistance of alumina coatings depends on the cohesive strength of deposited particles rather than on the density and/or hardness of the coating.[18] Tong et al. have shown that adhesive wear of plasma-sprayed WC-Co and Cr_2O_3 coating materials is proportional to the extension of a median crack. It was assumed that the lateral cracks had already formed, and the relationship of the wear rate of coating materials to the normal load follows a 2/3 power law instead of 9/8 for ceramic bulk materials.[19]

The purpose of the present work was to clarify the relationship between the properties of coatings, particularly the intersplat cohesive strength that can be measured by a simple bonding test, and wear mechanisms such as abrasive and adhesive wear and particle erosion.

Key Words: Cohesive strength, erosion behavior, material properties, WC-Co coatings, wear behavior

H.J. Kim, Y.G. Kweon, and R.W. Chang, Research Institute of Industrial Science and Technology, Welding Center, P.O. Box 135, Pohang, 790-600, Korea.

2. Experimental Details

2.1 *Coating Materials*

WC-12Co powder (Metco 71VF-NS) was used in these experiments. Table 1 summarizes the main characteristics of this powder. The morphology and a polished cross section of this starting powder are shown in Fig. 1. The substrate material for all coatings was low-carbon steel with a hardness of 195 HV.

2.2 *Spraying Process*

Air plasma spraying was conducted with the Metco 9MR system using argon and hydrogen as plasma gases. All specimens were grit blasted with alumina and then preheated to 100 °C just prior to thermal spraying. Spray rate (53 to 68 g/min) and spray distance (70 to 100 mm) were the principal parameters that were varied to obtain the different cohesive strength of the coatings. The coating thickness of 110 to 130 μm was obtained by multiple passes of the plasma torch to minimize thickness effects on the bonding test.[20]

2.3 *Bonding Test*

Bonding tests of each coating sample were made using a Sebastian IV coating adherence tester (Quad). The maximum strength of epoxy used was 1000 kg/cm^2 (98 MPa). The contact area of bonding was 5.7 mm^2, and the epoxy was cured in the

Table 1 Starting powder characteristics

Nominal composition	12.0 Co, 4.0 C, 1.0 Fe, 83.0 W
Manufacturing process	Fused and crushed
Particle size, μm	5-45

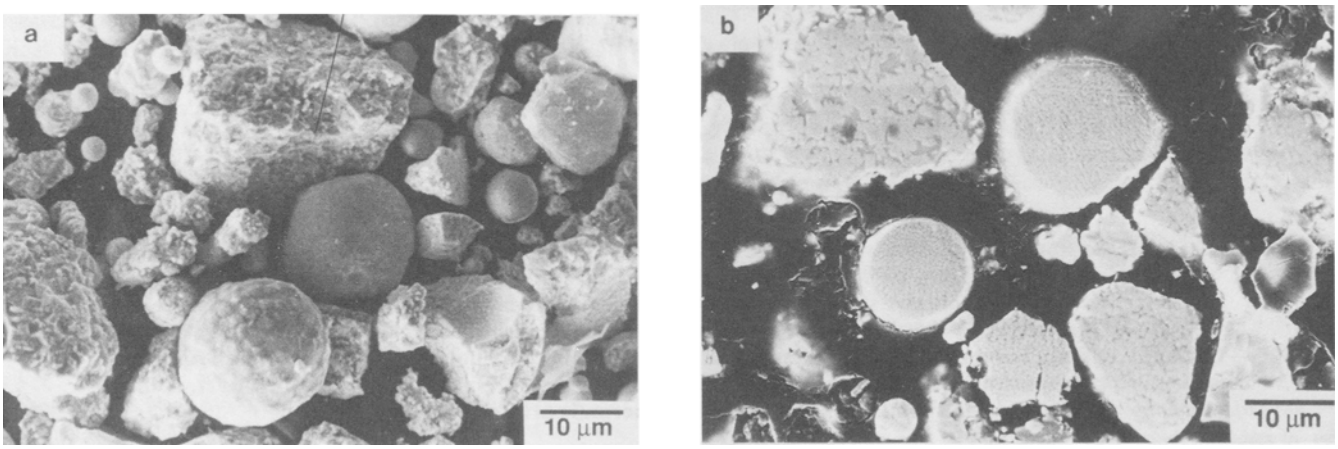

Fig. 1 Feedstock powders of WC-12Co plasma spray material. (a) As-received powder morphology. (b) Cross-sectional view of as-received powders

furnace for 70 min at 150 °C. The bond strength of the coating represents the average of five measurements.

2.4 *Wear Tests*

Abrasive wear resistance was evaluated using dry sand rubber wheel (DSRW) test equipment (ASTM G-65). Beach sand sieved to 212 to 300 μm was used instead of Ottawa standard sand. The morphology of the test sand is shown in Fig. 2(a). Preliminary test results showed approximately 5 to 10% lower wear volumes than those of the reference materials, possibly because of a low sand feeding rate (200 g/min). Test procedures, unless otherwise mentioned, were in accordance with ASTM Specification Procedure B. All abrasive wear tests were carried out on as-sprayed surfaces.

Adhesive wear tests were conducted with an EFM-III wear test machine (Orientec) using a ring-on-square arrangement with the coated square rotating against the steel ring in air at room temperature without lubrication. The mating material was quenched and tempered 0.45% carbon steel (330HV) and ground to approximately $R_a = 0.1$ μm, $R_t = 1$ μm. All of the adhesive tests were performed at the rotating speed of 200 rpm, and the applied load was 20 kg. The sliding velocity at the center of contact surfaces was 0.24 m/s, and the total contact area was 2 cm^2. Coatings were ground to approximately $R_a = 3.5$ μm and $R_t = 25$ μm before adhesive tests.

Erosion tests were performed using a modified grit blast unit. Test samples were positioned 30 mm away from the grit blast nozzle, and then alumina grit (45 to 90 μm in diameter) was accelerated by a flow of compressed air onto the surface of the test sample. The morphology of the erodent is also shown in Fig. 2(b). The velocity of the erodent particles, as measured by a rotating double-disk method,[21] was 32 m/s. Test surfaces were lightly blasted, prior to testing, to remove any oxidized surface present on the specimen.

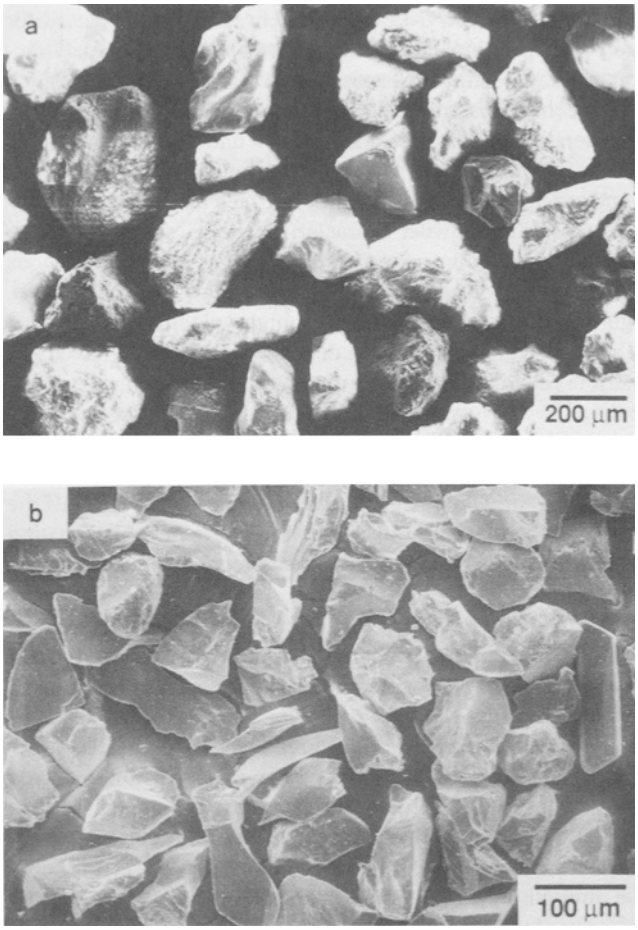

Fig. 2 Morphologies of wear test particles. (a) Beach sand for dry sand rubber wheel (DSRW) abrasive wear test (212 to 300 μm). (b) Alumina for erosion test (45 to 90 μm).

2.5 *Metallographic Evaluation*

All samples were sectioned with a low-speed diamond saw and cold epoxy mounted. Grinding and polishing operations were performed using a 40-μm bonded diamond platen until plane and then fine polished with diamond suspensions to minimize the likelihood of smearing or pullout.[22] The cross-sectional microhardness of the coatings was measured with a Matsuza DMH-1L Vickers hardness tester under a 200-g load. The average value of ten measurements was taken as the hardness of the sample. Porosity (% area) measurements were made using a computer-based image analysis system (Luzex 500) by analyzing 20 fields at a magnification of 600× on each sample. Surface

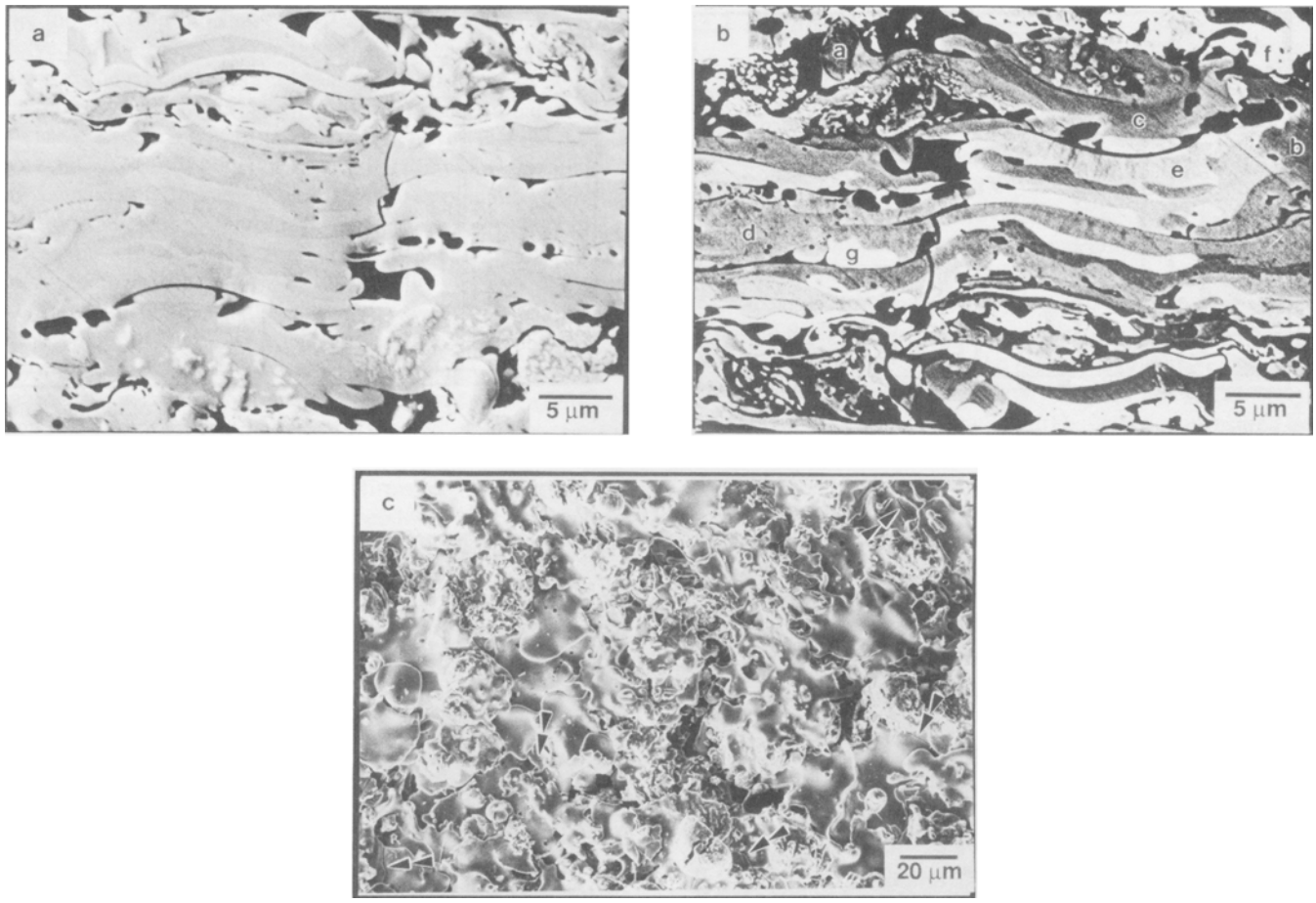

Fig. 3 Micrographs of plasma-sprayed WC-12Co coating. (a) Secondary electron image. (b) Back-scattering electron image of (a). (c) As-sprayed surface morphology.

Table 2 Chemical composition of each splat shown in Fig. 3(b)

Specimen	Composition, wt% W	Co	C	O	Fe
a	84.67	1.18	14.36	0.28	0.01
b	81.74	13.69	4.21	0.29	0.08
c	81.60	14.84	3.35	0.13	0.08
d	89.27	5.92	4.56	0.22	0.03
e	92.29	3.02	4.62	0.06	0.02
f	95.99	1.51	2.45	0.05	0.01
g	91.72	4.31	3.49	0.45	0.04

Table 3 X-ray relative intensities from starting powders and plasma sprayed WC-12Co coating

Specimen	W	WC	W_2C
Powder	...	100	70
Coating A	100	17	55
Coating B	100	45	92
Coating C	100	21	58
Coating D	89	61	100

roughness was measured using a Mitutoyo SurfTest 501 analytical profilometer equipped with an analyzer and recorder.

X-ray diffraction, auger scanning electron microscopy, carbon/sulfur determination, optical microscopy, STEM (200 KeV), and SEM (JEOL JXA-8600) equipped with wavelength-dispersive X-ray analysis (WDS), and energy-dispersive X-ray analysis (EDS) were used to characterize the powder, coatings, and wear tested specimens.

3. Results and Discussion

3.1 *Phase Characterization of Coatings*

Typical cross-sectional microstructures and as-sprayed surface morphologies are shown in Fig. 3. The cross sections show

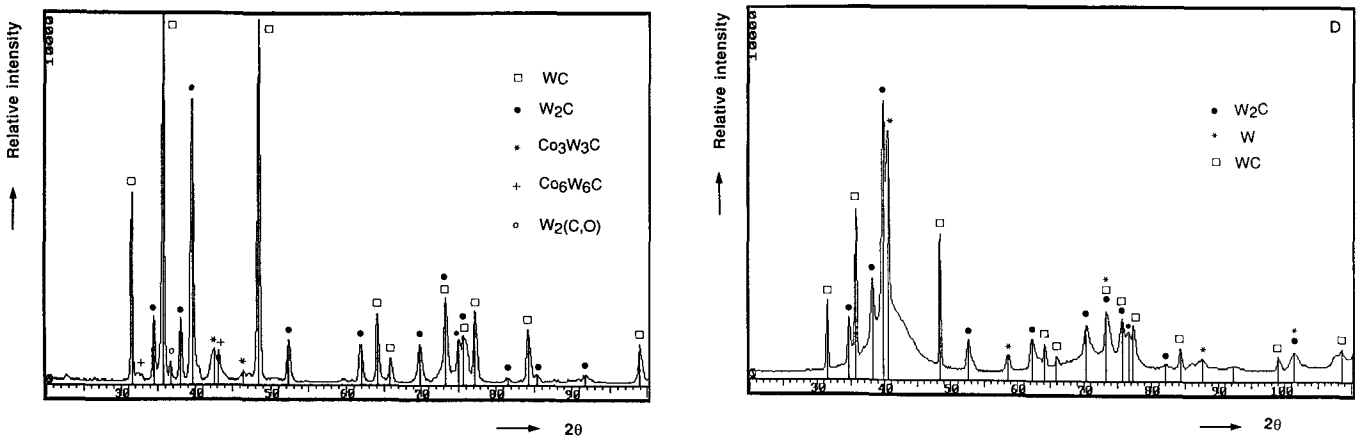

Fig. 4 X-ray diffraction patterns. (a) WC-12Co starting powder. (b) Typical air plasma sprayed WC-12Co coating.

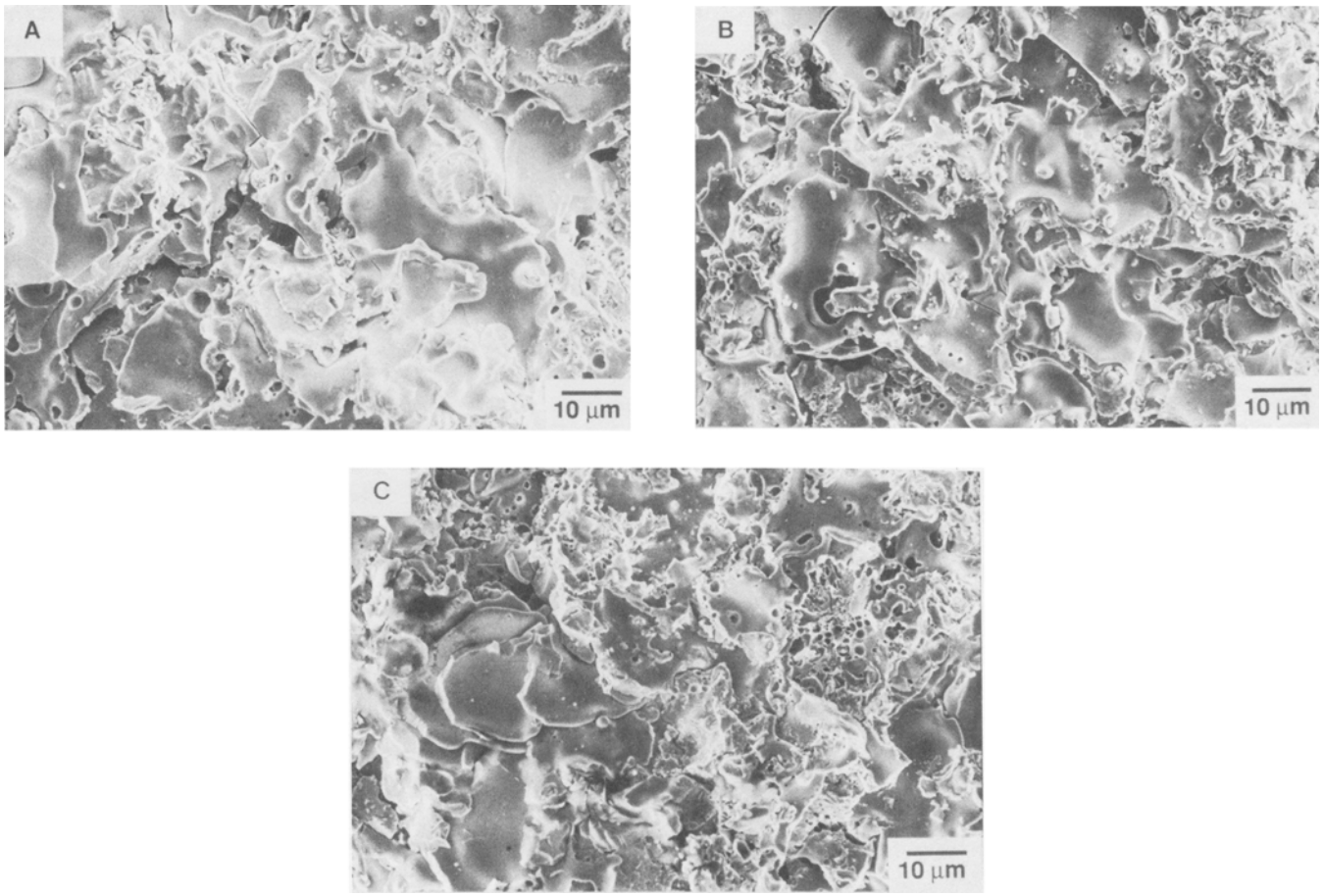

Fig. 5 Fracture surface from the bond strength test. (a) Coating A of cohesive strength of 551 kg/cm^2 (54 MPa). (b) Coating B of cohesive strength of 734 kg/cm^2 (72 MPa). (c) Coating D of cohesive strength of 892 kg/cm^2 (87 MPa).

not only porosity, unmelted particles, and retained carbides, but also transverse cracks that are normal to the interfaces between the lamellae. The SEM examination of the as-sprayed surface of the coatings also shows a network of fine cracks (indicated by the three sets of arrows in the lower portion of the photographs) perpendicular to the lamellar plane (Fig. 3c). The EPMA results from Fig. 3(b) are given in Table 2. The alphabetical codes (a to g) on Fig. 3(b) correspond to the rows shown in Table 2. The analysis area of the coating is at least 1 μm^2. Region a is the darkest, and there is a progression to the bright g region. Oxides of cobalt and tungsten are negligible in the coating. It is assumed that most of the iron and some of the cobalt was vaporized dur-

ing the spraying process.[8,10] Also, much of the tungsten dissolved in the matrix rather than forming carbide phases. Regions b and c appear darker because of higher cobalt contents; therefore, splats appear brighter as the tungsten content is increased. Based on EPMA results, it is believed that the thermal sprayed WC-Co coating is composed of individual lamella with different chemical compositions, as well as unmelted particles, porosity, and retained carbides. The coatings also contain many transverse and lateral cracks that are typical of thermal spray ceramic coatings.

X-ray diffraction analyses of the powder and coating are shown in Fig. 4 and Table 3. The feedstock powder contains substantial quantities of W_2C. This is expected because of the low initial carbon content of this powder (4.3 wt%). X-ray diffraction peaks from the coating (Fig. 4b) showed a broad maxima in the 38 to 46 2θ range that is characteristic of amorphous material. Bright-field TEM analysis confirms that the coating consists of crystalline particles embedded in an amorphous matrix.[23] It has been also reported that cobalt and excess carbon are present in the coating in an amorphous state due to rapid cooling during the spraying process.[23] X-ray diffraction did not reveal the presence of any significant amount of cobalt-containing subcarbides in the as-sprayed coatings, i.e., Co_3W_3C, Co_6W_6C, Co_2W_4C, etc. It is believed that more carbides are retained in Coating D, although this analysis is not quantitative.

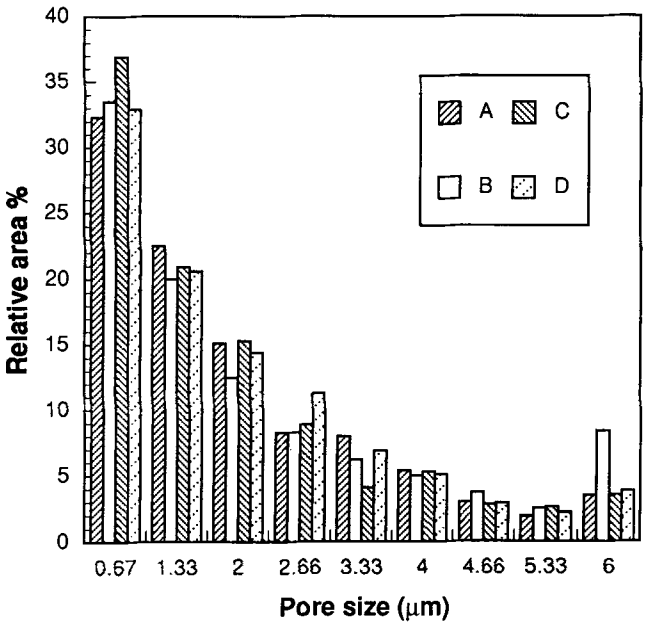

Fig. 6 Porosity distribution of plasma-sprayed WC-12Co coating.

3.2 *Bonding Test Properties*

Fracture surfaces after the bonding test are shown in Fig. 5. All failure occurred within the coating rather than at the coating/substrate interface when examined under 100× magnification. Therefore, it is believed that the measured strength is purely the cohesive strength of the deposited splat rather than the adhesive strength of the coating. The lower the cohesive strength, the more brittle fracture morphology along lamellar boundaries, i.e., compare Fig. 5(a) to Fig. 5(c).

Various coating properties are given in Table 4. It was not possible to determine the volume fraction of tungsten carbide and to quantify individual splat morphology of the coating surface by the computer image analysis techniques. The weight percentage of the retained carbon in coatings was measured by a combustion method, as reported in Table 4. As expected, the amount of decarburization is greater than 50% in all coatings, and the variation in microhardness is approximately 100 HV from the average due to inhomogeneity of the coating. It is reasonable to assume that all the coatings except B have almost the same hardness, porosity, and surface roughness. The proportion of pore sizes less than 1.3 μm is greater than 50% in all coatings. The B coating exhibits high porosity because of a significant proportion of large pores (Fig. 6). The difference between Coatings C and D is the amount of retained carbides (Table 3). Coating C has more dissolved excess carbon in the matrix because less decarburization has occurred relative to Coating D.

3.3 *DSRW Abrasive Wear Test*

Surface morphologies after DSRW wear tests are shown in Fig. 7. Surface inspection of the worn coating shows a flattening of protuberances due to the grinding action, but the prime feature is the large number of scattered cavities and defects. The main surface damage arises because of flat, plate-like chips that formed via a delamination mechanism. Chip formation by delamination derives from the development of subsurface microcracks. The cracks propagate parallel to the surface at a depth governed by the material properties and the manner of loading.[24] As mentioned in the Introduction, the extension of the transverse crack is the controlling factor for the coating removal process, and this follows a two thirds power law with normal load.[19] Therefore, the principal material factor for the coating removal process in the identical normal load condition is the intersplat cohesive strength of the coating.

In contrast, the wear mechanisms of Coating D are selective removal of the matrix followed by the removal of carbide grains. This is very similar to the wear mechanisms of sintered WC-Co alloy.[25] However, because the cohesive strength of the coating is decreased, the quantity and size of cavities and defects that

Table 4 Properties of atmospheric plasma-sprayed WC-12Co coating

Sample	Bond strength, kg/cm²	Carbon, wt%	Microhardness (HV200)	Surface roughness, μm As-sprayed	Surface roughness, μm After grinding	Porosity Area, %	Porosity Mean pore size, μm
A	588 (551 to 619)	1.62	873 (787 to 985)	4.63	3.35	3.87	2.19
B	757 (716 to 822)	1.97	739 (671 to 821)	5.18	3.61	8.03	2.51
C	884 (832 to 927)	2.11	840 (752 to 946)	4.71	3.88	3.78	2.07
D	886 (812 to 934)	2.05	842 (742 to 951)	4.47	3.58	4.91	2.21

Table 5 Comparison of chemical composition from Auger electron surface analysis before and after DSRW abrasive wear test at indicated sputtering depth

Sample		Composition, wt% Before test 70 Å	Before test 140 Å	After test 70 Å	After test 140 Å
A	W	84.5	89.7	76.0	85.1
	C	3.5	2.6	4.7	3.1
	O	2.3	1.7	4.3	2.9
	Co	9.8	6.1	15.0	9.0
B	W	...	...	83.2	87.8
	C	...	...	3.6	2.6
	O	...	...	3.4	2.3
	Co	...	...	9.8	7.3
C	W	89.1	90.7	77.5	85.3
	C	3.0	2.5	3.8	2.9
	O	1.4	1.0	3.7	2.2
	Co	6.4	5.8	15.0	9.6
D	W	89.5	91.2	83.6	85.0
	C	3.0	2.6	3.6	3.3
	O	1.0	0.7	3.8	3.2
	Co	6.6	5.4	9.1	8.5

Table 6 Abrasive and adhesive wear test results for plasma-sprayed WC-12Co coating

Sample	DSRW wear rate, mg/min	Ring-on-square: Coating loss, mg/h	Coating surface analysis, wt%	Steel loss, mg/h	Steel surface analysis, wt%	Friction coefficient Average	Friction coefficient Range
A	18.1	38.4	1.6 Fe	13.5	44.4 Fe	2.09	1.96-2.18
	18.7		8.7 Co		3.2 Co		
	18.9		89.7 W		52.4 W		
B	9.8	24.7	3.4 Fe	26.9	58.4 Fe	2.03	1.94-2.10
	10.5		10.0 Co		2.4 Co		
	10.9		86.6 W		39.1 W		
C	8.5	4.6	9.5 Fe	67.2	92.9 Fe	1.78	1.70-2.09
	8.6		9.5 Co		0.4 Co		
	8.7		81.0 W		6.5 W		
D	8.0	0.4	18.2 Fe	60.1	98.4 Fe	1.72	1.55-1.84
	8.1		8.2 Co		0.4 Co		
	8.2		73.7 W		1.5 W		

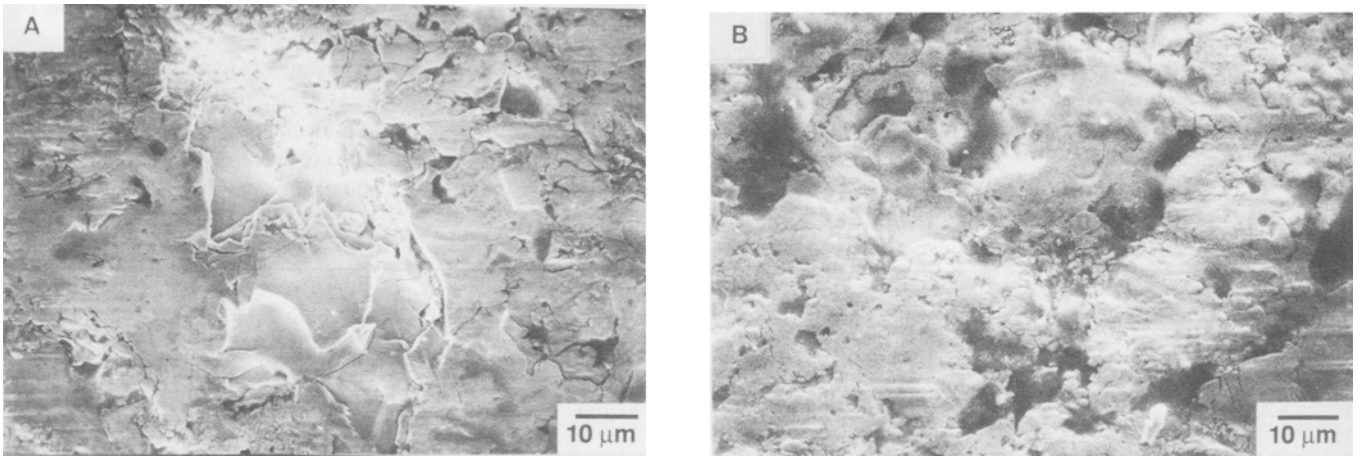

Fig. 7 Dry sand rubber wheel abrasive wear tested surface morphologies. (a) Material A. (b) Material D

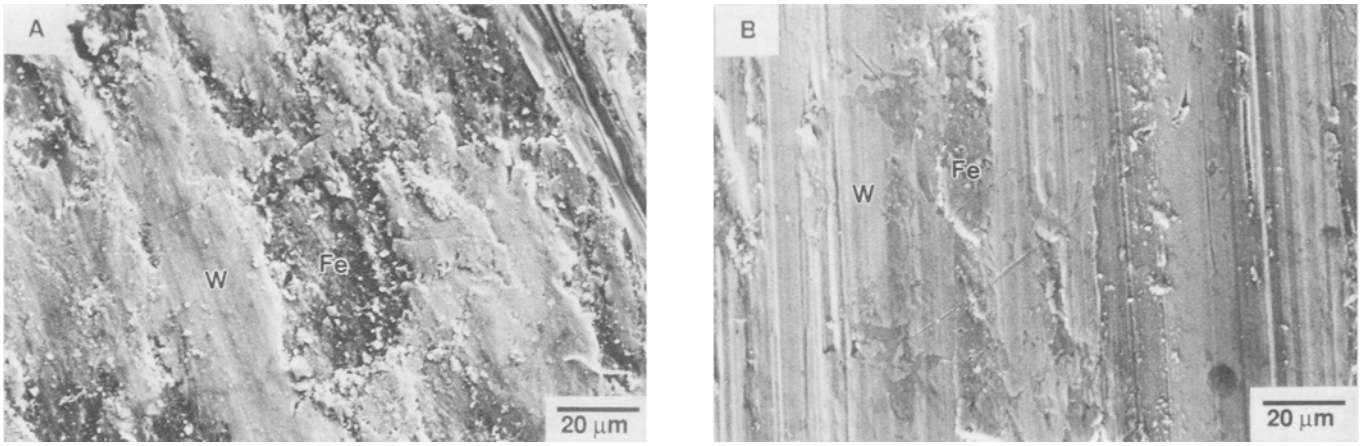

Fig. 8 Surface morphologies of the counterpart steel ring for ring-on-square adhesive wear test. (a) Material A. (b) Material D

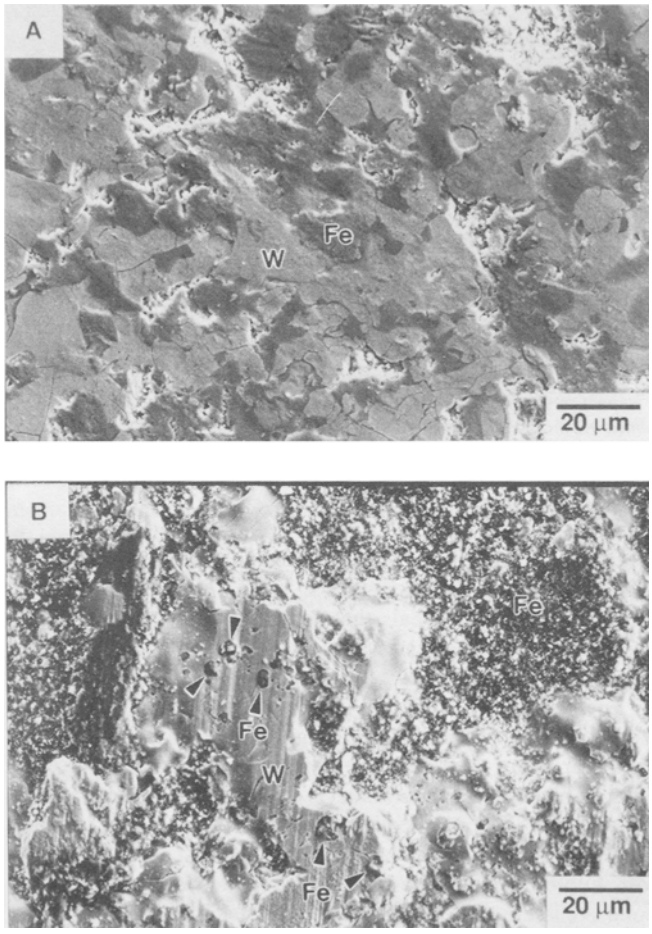

Fig. 9 Surface morphologies of ring-on-square adhesive wear test. (a) Material A. (b) Material D

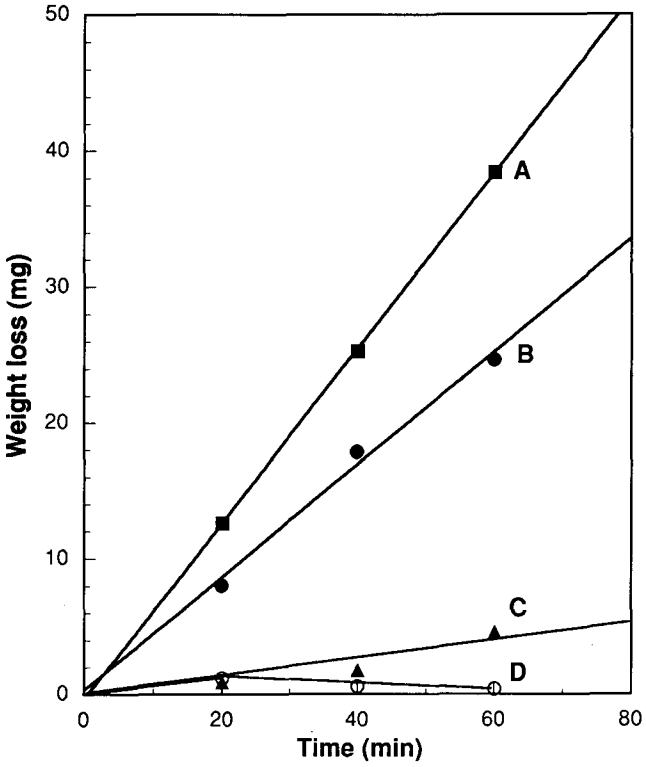

Fig. 10 Weight loss with time from ring-on-square adhesive wear test.

have derived from lamellar brittle fracture along individual splat boundaries is increased.

Auger electron surface analysis was conducted before and after the DSRW wear test to assess the compositional change due to the wear test (Table 5). The analysis was made after 70 and 140 Å sputtering to eliminate the possible oxide layers that were always present. The atomic percentage value derived from this analysis was converted to a weight percentage. The data for Coating B before the wear test were excluded because this coating exhibited many other impurities. It can be seen in Table 5 that, as the sputtering depth is increased from 70 to 140 Å, the amount of W is increased, but the amounts of C, O, and Co are decreased. It is assumed that Co was selectively sputtered and that the oxide layer was still present above 70 Å. After the wear test, the opposite reaction occurs, i.e., the amount of W decreases and the amounts of C, O, and Co increased. This indicates the presence of cobalt oxide due to the wear test, although

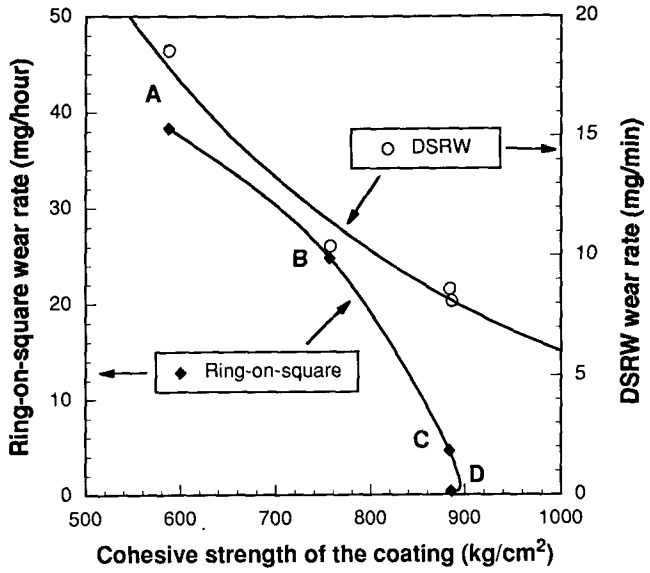

Fig. 11 Results of wear rate on cohesive strength of the coating

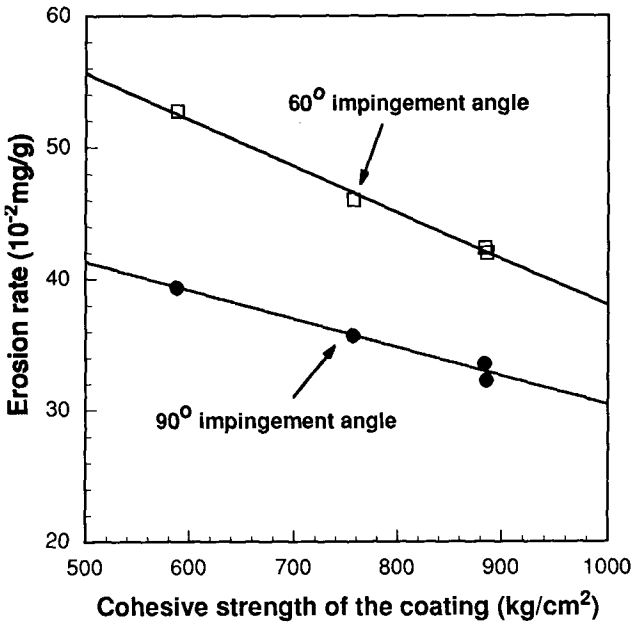

Fig. 12 Erosion wear rate showing dependence on the cohesive strength of the coating

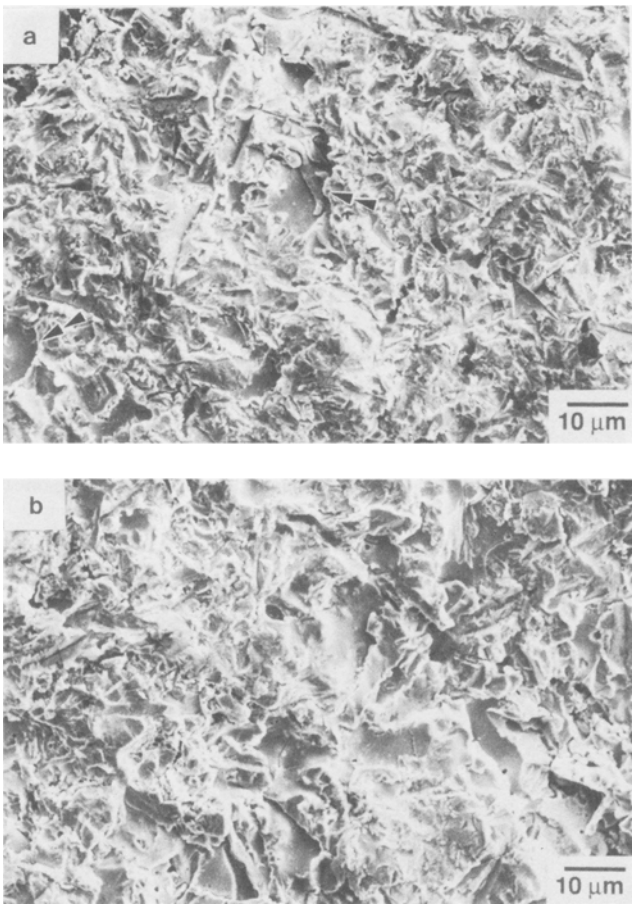

Fig. 13 Erosion scar of plasma-sprayed WC-12Co coating. (a) 90° impact of specimen B. (b) 60° impact of specimen B. The arrow in the mid-view of (a) indicates either fracture at a splat boundary or fracture that is associated with porosity.

the oxidation phenomenon is not severe. Other researchers have reported the presence of a free carbon surface film after wear testing.[17,26] The increase in carbon may be an indication of a carbon surface film, although the carbon increase is not significant enough to be included in the experimental error.

3.4 *Ring-on-Square Adhesive Wear Test*

Results of abrasive and adhesive wear tests are presented in Table 6. As the adhesive wear resistance increases, the friction coefficient—both the average and the range—decreases. However, weight loss of the counterpart steel increases. Friction coefficients that are higher than reported values are probably due to higher initial surface roughness.[17,27,28] The EDS analysis of steel surfaces also reveals that more WC-Co coating has adhered to the steel surface as the cohesive strength of the coating decreases.

For example, less coating D adheres to the steel surface. Instead, the steel surface exhibits significant scratching (Fig. 8). However, more wear debris remained on the coating side even after air blasting, and some steel is embedded in the coating surface (Fig. 9). This resulted in a weight gain as the wear test proceeded (Fig. 10). Other coatings exhibit almost constant weight loss with time. More coating adheres to the steel surface as the cohesive strength of the coating decreases. This results in wear between the hard WC-Co coating pair rather than between the steel/coating pair. Therefore, the dominant wear mechanism is adhesion rather than oxidation and/or abrasion for low cohesive strength coatings. It has been mentioned that material transfer between a hard ceramic coating and metal depends on the load and on the temperature at the interface.[27] Again, the dominant material property of the coating for adhesion is the intersplat cohesive strength, assuming that the test conditions are similar.

Dependence of abrasive and adhesive wear rates on the cohesive strength of the coating is shown in Fig. 11. Even though

coating A has the highest hardness, it exhibits the poorest wear performance. The low porosity and hardness and higher retained carbide effects of coating B on wear are masked by the low cohesive strength effect. The slightly better wear performance of coating D compared to coating C may arise from the higher percentage of retained carbides in the coating, although coating D has lower porosity.

3.5 *Solid Particle Erosion*

Figure 12 shows the alumina particle erosion rate with respect to the cohesive strength of the coating. A linear relationship exists with respect to the cohesive strength of the coating. Although it is not conclusive, ductile erosion behavior occurs that increases the erosion rate as the impingement angle decreases. Alumina particles embedded on the eroded surface were also detected by EDS analysis.

It has been suggested that microchipping and ploughing, debonding at splat boundaries, and splat fracture associated with porosity are three basic mechanisms of material removal processes for thermal sprayed materials.[29] It is difficult to differentiate between the splat boundary fracture and splat fracture associated with porosity (Fig. 13). However, the results of the present work indicate that debonding at the splat boundary is the dominant mechanism governing the erosion rate of the coating materials. As the impact angle is decreased, splat fracture and/or debonding mechanisms at splat boundaries are increased (Fig. 13). It is suspected that the very angular shape of the alumina erodent causes the wedge effect at low impact angle.

4. Conclusion

This study on wear mechanisms such as abrasion, adhesion, and particle erosion was performed to clarify the relationship with coating properties and can be summarized as follows. Atmospheric plasma-sprayed WC-12%Co coatings are composed of individual splats with different chemical compositions as well as unmelted particles, porosity, retained carbides, and many transverse and lateral cracks. Porosity, hardness, surface roughness, and retained carbide of the coatings are not the principal factors for wear performance. The cohesive strength of the thermal spray coating is the most important factor affecting the wear performance of the material. As the cohesive strength of the coating increases, the wear resistance to abrasive, adhesive, and particle erosion also increases.

References

1. T.C. Nerz, J.E. Nerz, B.A. Kushner, A.J. Rotolico, and W.L. Riggs, Evaluation of HEP Sprayed Tungsten Carbide/Cobalt Coating Using Design of Experiment Method, *Thermal Spray: International Advances in Coatings Technology*, C.C. Berndt, Ed., ASM International, 1992, p 405-414
2. K. Niemi, P. Vuoristo, T. Mantyla, G. Barbezat, and A.R. Nicoll, Abrasion Wear Resistance of Carbide Coatings Deposited by Plasma and High Velocity Combustion Processes, *Thermal Spray: International Advances in Coatings Technology*, C.C. Berndt, Ed., ASM International, 1992, p 685-689
3. B. Dulin and A.R. Nicoll, Plasma Sprayed Tungsten Carbide-Cobalt Coating, *Thermal Spray: Advances in Coatings Technology*, D.L. Houck, Ed., ASM International, 1988, p 345-351
4. X. Quo, H. Herman, and S. Rangaswamy, Cavitation-Erosion of Plasma-Sprayed WC-Co, *Advances in Thermal Spraying*, Pergamon Press, 1986, p 37-46
5. S. Rangaswamy and H. Herman, Metallurgical Characterization of Plasma Sprayed WC-Co Coatings, *Advances in Thermal Spraying*, Pergamon Press, 1986, p 101-110
6. H. Kreye, D. Fandrich, H.-H. Muller, and G. Reiners, Microstructure and Bond Strength of WC-Co Coatings Deposited by Hypersonic Flame Spraying, *Advances in Thermal Spraying*, Pergamon Press, 1986, p 121-128
7. Y. Arata, A. Ohmori, and E. Gofuku, Studies on WC-Co System Coatings by High Energy Thermal Spraying, *Advances in Thermal Spraying*, Pergamon Press, 1986, p 805-813
8. J. Subrahmanyam, M.P. Srivastava, and R. Sivakumar, Characterization of Plasma-Sprayed WC-Co Coatings, *Mater. Sci. Eng.*, Vol 84, 1986, p 209-214
9. V. Ramnath and N. Jayaraman, Characterization and Wear Performances of Plasma Sprayed WC-Co Coatings, *Mater. Sci. Technol.*, Vol 5, 1989, p 382-388
10. D. Tu, S. Chang, C. Chao, and C. Lin, Tungsten Carbide Phase Transformation during the Plasma Spray Process, *J. Vac. Sci. Technol.*, Vol A3 (No. 6), 1985, p 2479-2482
11. M.E. Vinayo, F. Kassabji, J. Guyonnet, and P. Fauchais, Plasma Sprayed WC-Co Coatings: Influence of Spray Conditions (Atmospheric and Low Pressure Plasma Spraying) on the Crystal Structure, Porosity, and Hardness, *J. Vac. Sci. Technol.*, Vol A3 (No. 6), 1985, p 2483-2489
12. Y.A. Kharlamov, Detonation Spraying of Protective Coatings, *Mater. Sci. Eng.*, Vol 93, 1987, p 1-37
13. T.P. Slavin and T. Nerz, Material Characteristics and Performance of WC-Co Wear-Resistant Coatings, *Thermal Spray Research and Applications*, T.F. Bernecki, Ed., ASM International, 1991, p 159-164
14. I. Nogueira, A. Ramalho, A. Morao Dias, and A. Gonealves, Friction and Wear Performance of Plasma Sprayed Cr_2O_3 Coatings, *Thermal Spray: International Advances in Coatings Technology*, C.C. Berndt, Ed., ASM International, 1992, p 717-722
15. R.W. Smith, D. Gentner, E. Harzenski, and T. Robisch, The Structure and Properties of Plasma Sprayed TiC Dispersion Hardened Coatings, *Thermal Spray Technology—New Ideas and Processes*, D.L. Houck, Ed., ASM International, 1989, p 299-306
16. M. Scholl and P. Claton, Abrasive and Erosive Wear of Some Hypervelocity Air Plasma Sprayed Coating, *Thermal Sprayed Coatings: Properties, Processes, and Applications*, T.F. Bernecki, Ed., ASM International, 1992, p 39-52
17. M. Cartier, L. McDonnell, and E.M. Cashell, Friction of Tungsten Carbide-Cobalt Coatings Obtained by Means of Plasma Spraying, *Surf. Coat. Technol.*, Vol 48, 1991, p 241-248
18. K. Furukubo, S. Oki, and S. Gohda, Relationship between Wear and Microstructures of Ceramic Spray Coatings, *Thermal Spray: International Advances in Coatings Technology*, C.C. Berndt, Ed., ASM International, 1992, p 705-709
19. T. Zhhaohe, D. Chuanxian, and Y. Dongsheng, A Fracture Model for Wear Mechanism in Plasma Sprayed Ceramic Coating Materials, *Wear*, Vol 155, 1992, p 309-316
20. Y. Shimizu, M. Sato, M. Kobayashi, and K. Maeda, Effect of Test Specimen Size upon Adhesive Strength of Flame Sprayed Coatings, *Thermal Sprayed Coatings: Properties, Processes, and Applications*, T.F. Bernecki, Ed., ASM International, 1992, p 257-262
21. A.W. Ruff and L.K. Ives, Measurement of Solid Particle Velocity in Erosive Wear, *Wear*, Vol 35, 1975, p 195-199
22. M.F. Smith, D.T. McGuffin, J.A. Henfling, and W.B. Lenling, A Comparison of Techniques for the Metallographic Preparation of Thermal Sprayed Samples, *Thermal Sprayed Coatings: Properties, Processes, and Applications*, T.F. Bernecki, Ed., ASM International, 1992, p 97-104

23. J.E. Nerz, B.A. Kushner, Jr., and A.J. Rotolico, Microstructural Evaluation of Tungsten Carbide-Cobalt Coatings, *Thermal Sprayed Coatings: Properties, Processes, and Applications*, T.F. Bernecki, Ed., ASM International, 1992, p 115-120
24. M. Boas and M. Bamberger, Low Load Abrasive Wear Behavior of Plasma Sprayed and Laser-Melted Plasma Coatings, *Wear*, Vol 126, 1988, p 197-210
25. J. Larsen-Basse, Binder Extrusion in Sliding Wear of WC-Co Alloys, *Wear*, Vol 105, 1985, p 247-256
26. S.E. Franklin and J. Beuger, A Comparison of the Tribological Behavior of Several Wear-Resistant Coatings, *Surf. Coat. Technol.*, Vol 54/55, 1992, p 459-465
27. A. Tronche and P. Fauchais, Frictional Behavior against Steel of Aluminium Substrates Plasma Sprayed with Hard Coatings, *Mater. Sci. Eng. A*, Vol 102, 1988, p 1-12
28. A. Tronche and P. Fauchais, Hard Coatings (Cr_2O_3, WC-Co) Properties on Aluminium or Steel Substrates, *Mater. Sci. Eng.*, Vol 92, 1987, p 133-144
29. R. Kingswell, D.S. Rickerby, K.T. Scott, and S.J. Bull, Comparison of the Erosive Wear Behavior of Vacuum Plasma Sprayed and Bulk Alumina, *Thermal Spray Research and Applications*, T.F. Bernecki, Ed., ASM International, 1991, p 179-185